Computational and Experimental Studies of (2,2)-Bis(indol-1-yl-methyl)acetate Suggest the Importance of the Hydrophobic Effect in Aromatic Stacking Interactions

Yuan-Ping Pang,[†] Jennifer L. Miller,[‡] and Peter A. Kollman*

Contribution from the Department of Pharmaceutical Chemistry, School of Pharmacy, University of California, San Francisco, California 94143

Received August 10, 1998

Abstract: To understand the driving forces of aromatic stacking interactions in water, we have performed conformational searches, molecular dynamics simulations, potential of mean force (PMF) and free energy perturbation (FEP) calculations, syntheses, and NMR studies on sodium (2,2)-bis(indol-1-yl-methyl)acetate (**1**), sodium 3-indol-1-yl-2-methyl-propionate (**2**), and sodium 3-indol-1-yl-propionate (**3**). The conformational searches on **1** revealed that the isobutyric acid linker of **1** allows the molecule to adopt the tilted T-shaped stacked, off-center stacked, face-to-face stacked, and nonstacked conformations in a vacuum. The PMF and FEP calculations suggested that the most thermodynamically stable conformers in water are the tilted T-shaped stacked and nonstacked conformers. Independent NMR spectroscopic studies of **1**−**3** revealed that both the tilted T-shaped stacked and nonstacked conformers are populated in D_2O and in d_6-DMSO, and they are in a rapid equilibrium. Furthermore, the NMR studies found (i) a larger population of the tilted T-shaped stacked conformation of **1** at 22 °C in D_2O than in d_6-DMSO and (ii) more different populated stacked conformations of **1** at 60 °C in D_2O than in d_6-DMSO. One would expect larger populations of the stacked conformations in d_6-DMSO, whose dielectric constant is smaller than that of water, if the electrostatic interaction were the only driving force of the aromatic stacking interactions. The results, therefore, suggest that the hydrophobic effect plays an important role in the stacking interaction of **1** in water.

Introduction

Interactions between aromatic functional groups play a role in folding and complexation of biopolymers.[1,2] In particular, aromatic interactions are closely associated with the stabilization of nucleic acid structures and the intercalation of drugs into DNA and RNA. The stacking interactions of aromatic hydrocarbons such as benzene in water are usually attributed to the hydrophobic effect, namely, water's preference for interacting with itself relative to interacting with the aromatic hydrocarbons.[3] Similarly, the aromatic stacking interactions of heterocycles such as adenine in water have been suggested to be due to the hydrophobic effect, dispersion attractions, and attractive interactions between the partial charges on heterocycles.[4−8] On the other hand, it has been suggested that the aromatic stacking interactions stem exclusively from the attractive electrostatic interactions between heterocycles.[9−11] Inspired by the literature work of using propylene- or isobutyric acid-linked bis-heterocycles to probe the interactions between aromatic groups,[9−20] we have carried out computational and experimental studies of stacking interactions of a novel molecular probe, sodium (2,2)-bis(indol-1-yl-methyl)acetate (**1**, Figure 1) in water and in DMSO to investigate the role of the hydrophobic effect in aromatic stacking interactions.

Strategy

We wanted to answer three questions through conformational searches, molecular dynamics (MD) simulations, potential of mean force (PMF) and free energy perturbation (FEP) calculations, syntheses, and NMR studies of **1** and its monomeric

* To whom correspondence and reprint requests should be addressed.
[†] On sabbatical leave from Neurochemistry Research, Mayo Foundation for Medical Education and Research, 4500 San Pablo Rd., Jacksonville, FL 32224. Current address: Department of Pharmacology, Mayo Foundation for Medical Education and Research, 200 First St. SW, Rochester, MN 55905.
[‡] Current address: CombiChem North, 1804 Embarcadero Rd., Suite 201, Palo Alto, CA 94303.

(1) Burley, S. K.; Petsko, G. A. *Adv. Protein Chem.* **1988**, *39*, 125.
(2) Saenger, W. *Principles of Nucleic Acid Structure*; Springer-Verlag: New York, 1984.
(3) Muller, N. *Acc. Chem. Res.* **1990**, *23*, 23.
(4) Ts'o, P. O. P. In *Basic Principles in Nucleic Acid Chemistry*; Ts'o, P. O. P., Ed.; Academic Press: New York, 1974; Vol. I.
(5) Crothers, D. M.; Ratner, D. I. *Biochemistry* **1968**, *7*, 1823.
(6) Ts'o, P. O. P.; Kondo, N. S.; Robins, R. K.; Broom, A. D. *J. Am. Chem. Soc.* **1969**, *91*, 5625.
(7) Tazawa, I.; Koike, T.; Inoue, Y. *Eur. J. Biochem.* **1980**, *109*, 33.
(8) Friedman, R. A.; Honig, B. *Biophys. J.* **1995**, *69*, 1528−1535.
(9) Newcomb, L. F.; Gellman, S. H. *J. Am. Chem. Soc.* **1994**, *116*, 4993−4994.
(10) Newcomb, L. F.; Haque, T. S.; Gellman, S. H. *J. Am. Chem. Soc.* **1995**, *117*, 6509−6519.
(11) Gellman, S. H.; Haque, T. S.; Newcomb, L. F. *Biophys. J.* **1996**, *71*, 3523−3525.
(12) Browne, D. T.; Eisinger, J.; Leonard, N. J. *J. Am. Chem. Soc.* **1968**, *90*, 7302−7323.
(13) Frank, J. K.; Paul, I. C. *J. Am. Chem. Soc.* **1973**, *95*, 2324−2332.
(14) Leonard, N. J.; Ito, K. *J. Am. Chem. Soc.* **1973**, *95*, 4010−4016.
(15) Leonard, N. J. *Acc. Chem. Res.* **1979**, *12*, 423.
(16) Constant, J. F.; Laugaa, P.; Roques, B. P.; Lhomme, J. *Biochemistry* **1988**, *27*, 3997−4003.
(17) Mutai, K.; Gruber, B. A.; Leonard, N. J. *J. Am. Chem. Soc.* **1975**, *97*, 4095−4104.
(18) Voet, D. *J. Am. Chem. Soc.* **1980**, *102*, 2071−2074.
(19) Ishida, T.; Shibata, M.; Fujii, K.; Inoue, M. *Biochemistry* **1983**, *22*, 3571−3581.
(20) Friedman, R. A.; Honig, B. *Biophys. J.* **1996**, *71*, 3525−3526.

10.1021/ja9828410 CCC: $18.00
Published on Web 02/10/1999

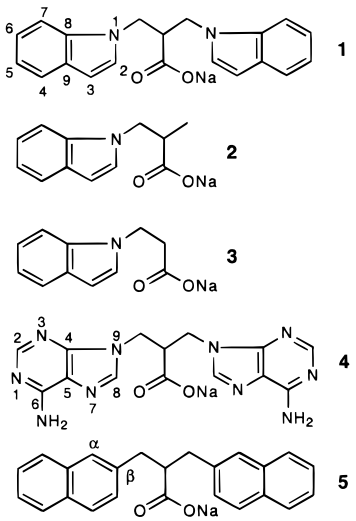

Figure 1. Chemical structures of **1**−**5**.

analogues (**2** and **3**, Figure 1). First, can **1** adopt the tilted T-shaped, off-center, and face-to-face stacked conformations?[21] Second, which stacked conformation(s) is preferred in water if **1** adopts a stacked conformation(s)? Third, does the hydrophobic effect play a role in the stacked conformations of **1**?

The reasons to investigate **1** are as follows: First, concerning the partial charges on the indole ring, **1** can be viewed as a hybrid of a heterocycle **4** (Figure 1) and an aromatic hydrocarbon **5** (Figure 1), which were found to adopt parallel stacked and nonstacked conformations in water, respectively.[9−11,20] Knowledge of stacking or nonstacking behavior of **1** in water can yield insights into the hydrophobic effect in aromatic stacking interactions. Second, **1** is readily synthetically accessible. Third, the seven proton signals of the indole ring are generally distinguishable in the NMR spectrum. This permits an analysis of upfield or downfield shifts of the indole protons that can yield crucial experimental evidence about the stacking or nonstacking behavior of **1** in water. Fourth, **1** can later be theoretically mutated to heterocycle **4** through steps, at each of which one carbon (or hydrogen) atom is changed to a nitrogen atom by employing a single-topology-based free energy perturbation approach.[22] This permits an investigation on which part of the partial charges on the adenine group plays a role in the aromatic stacking interactions of **4**. Although the aromatic hydrocarbon **5** can also be theoretically mutated to **4** using a dual-topology-based free energy perturbation approach for investigation of the charge contribution, it is more efficient to work with perturbations of **1** using the single-topology-based approach.[22−24]

To answer the three questions, we first performed conformational analysis of **1** to investigate if the commonly observed tilted T-shaped, off-center, and face-to-face stacked conformations are available to the isobutyric acid linked bis-indole **1**.[21] We then carried out MD simulations of **1** in water. This study did not provide information on relative conformational stability, and yet it yielded information on interconversions among different conformers derived from conformational searches. This information was later used in PMF calculations. To estimate

Table 1. Definition of the Six Torsions that Determine the Conformations of **1**

torsion	atom ID of **1**[a]
T1	14−15−16−19
T2	15−16−19−24
T3	28−27−24−19
T4	27−24−19−16
T5	27−24−19−21
T6	24−19−21−22

[a] For atom IDs, see Figure 4.

the relative conformational stabilities of **1** in water at 25 °C, we carried out PMF calculations, which compute the potential of mean force, characterizing conformational change as a function of the first four torsions specified in Table 1 with holonomic internal constraints.[25] To effectively evaluate the conformational stabilities of two conformers generated by exchanging the carboxylate group and the methine hydrogen atom of **1**, we used FEP calculations,[22] which compute the free energy difference between the two by perturbing the CO_2^- and H groups to one another. Use of the FEP calculations rather than the more computing-intensive PMF approach also simplified the conformational analysis of **1** because the relative orientations of the carboxylate group were no longer of concern. Both PMF and FEP calculations employing MD simulations were performed in a box of explicit water molecules (TIP3P)[26] with periodic boundary conditions, and thus they include the solvent and entropy effects on conformational stability. Such calculations are computing intensive and yet most appropriate, since the stacking interactions involve considerable enthalpy−entropy compensation. Evaluation with just potential energies of different conformations would omit the solvent and entropy effects and, therefore, not be able to assess the contribution of the hydrophobic effect.

We then launched synthesis and NMR spectroscopic studies on **1**−**3** to detect the populated conformations of **1** in water and in DMSO. The NMR studies were focused on (i) chemical shifts of the aromatic protons, which can provide information about the stacking and nonstacking interactions, (ii) coupling constants of the methylene protons, which can offer insights into determination of which conformations are not likely in water on the basis of torsions calculated from the observed coupling constants by the Karplus equation,[27] and (iii) symmetry information contained in the spectra, which provides insights into the conformational dynamics.

Results

Accuracy of the Computational Approach. The reliability and accuracy of our computational approach rely mainly on force field and sampling in the MD simulations.[22] For the force field, we used a well-balanced, second-generation AMBER force field.[28] This force field was developed specifically for the simulations in solution (TIP3P water molecules) and is most appropriate to the present work. Furthermore, Chipot et al. have reported a study of benzene stacking interaction in water by means of free energy calculations with the second-generation AMBER force field.[29] According to their calculations, the

(21) Hunter, C. A.; Sanders, K. M. *J. Am. Chem. Soc.* **1990**, *112*, 5525−5534.
(22) Kollman, P. *Chem. Rev.* **1993**, *93*, 2395−2417.
(23) Pearlman, D. A.; Case, D. A.; Caldwell, J. W.; Ross, W. S.; Cheatham III, T. E.; Debolt, S.; Ferguson, D.; Seibel, G.; Kollman, P. A. *Comput. Phys. Commun.* **1995**, *91*, 1−41.
(24) Sun, Y. C.; Veenstra, D. L.; Kollman, P. A. *Protein Eng.* **1996**, *9*, 273−281.
(25) Tobias, D. J.; Brooks, C. L. *J. Chem. Phys.* **1988**, *89*, 5115−5127.
(26) Jorgensen, W. L.; Chandreskhar, J.; Madura, J. D.; Impey, R. W.; Klein, M. L. *J. Chem. Phys.* **1982**, *79*, 926−935.
(27) Silverstein, R. M.; Bassler, G. C.; Morill, T. C. *Spectroscopic Identification of Organic Compounds*, 5th ed.; Wiley: New York, 1991; p 196.
(28) Cornell, W. D.; Cieplak, P.; Bayly, C. I.; Gould, I. R.; Merz, K. M., Jr.; Ferguson, D. M.; Spellmeyer, D. C.; Fox, T.; Caldwell, J. W.; Kollman, P. A. *J. Am. Chem. Soc.* **1995**, *117*, 5179−5197.

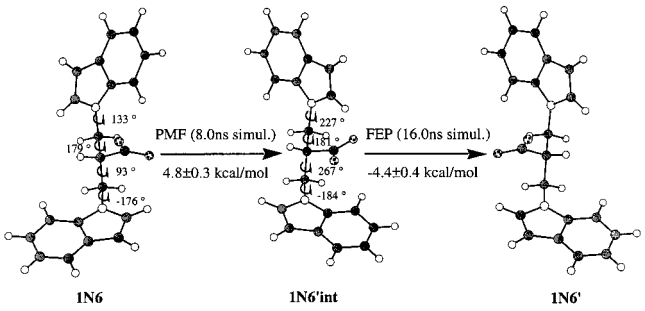

Figure 2. Conversion between the two mirror images through the PMF and FEP calculations.

parallel stacked benzene dimer has a contact and a solvent-separated minimum with corresponding free energies of association of −0.47 and −0.43 kcal/mol, respectively; the T-shaped benzene dimer has corresponding energies of −1.94 and −0.74 kcal/mol. These results are consistent with the report of other studies using an ab initio potential, which found free energies of −0.1 and −0.74 kcal/mol for the contact and the solvent-separated minima of the parallel benzene dimer, and −1.9 and −0.4 kcal/mol for the T-shaped benzene dimer.[30,31] They have also shown good agreement for isolated benzene−benzene interactions between the molecular mechanics calculations with the new AMBER force field and high-level ab initio calculations.[29] Chipot's results suggest that the new AMBER force field is reliable for prediction of aromatic interactions of **1**, which is structurally analogous to the benzene dimer. For the sampling, we carried out nanosecond scale MD simulations with two dedicated SGI supercomputers (Power Challenge with 4×R10K processors and Origin 2000 with 8×R10K processors), which allowed us to evaluate the convergence of the simulations.

To assess the inherent accuracy of the PMF and FEP methods, we performed a perturbation of one conformation of bis-indole **1** (**1N6**), through a large conformational change, to its thermodynamically identical mirror image (**1N6′**) by employing a PMF calculation to change the conformation of the linker (**1N6′int**), followed by a FEP calculation to exchange the carboxylate and methine proton (**1N6′**) (Figure 2). Using the combined PMF and FEP strategy, we found that the calculated free energy difference between the two mirror images was 0.4 ± 0.7 kcal/mol (see Materials and Methods). This result suggests that the combined PMF and FEP approach would be reliable in predicting preference of two conformers whose free energy difference is greater than 0.4 ± 0.7 kcal/mol.

The reliability of the free energy perturbation studies will be demonstrated later (i) by the closed thermodynamic cycle constructed by the calculated free energy changes (see PMF Calculations) and (ii) by the consistent, independent NMR results (see Populated Tilted T-Shaped Stacked Conformations and Populated Nonstacked Conformations).

Conformational Analysis. A total of 12 different conformers of **1** was identified from a conformational search of this molecule. Six torsions that define the 12 conformers are listed in Table 2. There are two tilted T-shaped conformers, two face-to-face stacked conformers, three off-center stacked conformers, and five nonstacked conformers (see Figure 3). According to the conformational search, the isobutyric acid linker does not prevent **1** from adopting the tilted T-shaped and other two parallel stacked conformations in a vacuum.

(29) Chipot, C.; Jaffe, R.; Maigret, B.; Pearlman, D. A.; Kollman, P. A. *J. Am. Chem. Soc.* **1996**, *118*, 11217−11224.
(30) Linse, P. *J. Am. Chem. Soc.* **1992**, *114*, 4366.
(31) Hobza, P.; Selzle, H. L.; Schlag, E. W. *J. Am. Chem. Soc.* **1994**, *116*, 3500−3506.

Table 2. Torsions (Deg of Arc) of the 12 Different Conformations of **1**

conformer[a]	description	T1	T2	T3	T4	T5	T6
1N1	nonstacked	92	−179	−96	177	−59	−61
1N2	nonstacked	104	−58	94	−170	65	−148
1F3	indolyl ring stacked	119	−74	−121	53	−80	0
1S4	phenyl ring stacked	118	−41	128	−55	177	46
1T5	T-shaped stacked	72	63	90	−175	62	42
1N6	nonstacked	−98	−174	−94	177	−60	130
1T7	T-shaped stacked	−104	67	93	−174	63	43
1N8	nonstacked	−97	177	−167	−176	60	70
1N9	nonstacked	94	65	−93	169	−66	152
1S10	pyrrolyl ring stacked	−66	−67	−122	72	−165	120
1O11	off-center stacked	71	60	−123	50	−78	95
1F12	indolyl ring stacked	65	78	−63	−58	179	63

[a] The letters N, F, S, T, and O indicate the nonstacked, face-to-face stacked, partial face-to-face stacked, tilted T-shaped stacked and off-center stacked conformations, respectively. For definitions of T1−T6, see Table 1 and Figure 4.

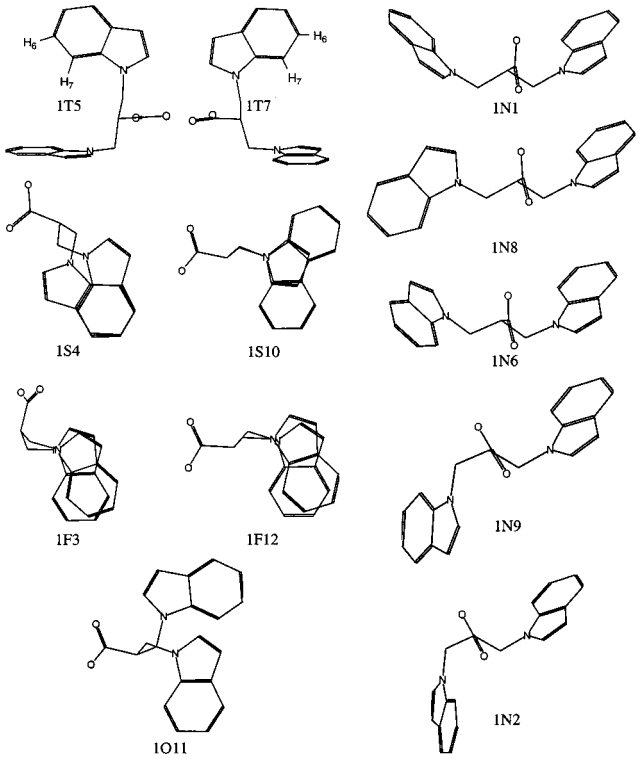

Figure 3. Conformations of **1** identified from the conformational search (H atoms, except for H^6 and H^7 in the tilted T-shaped conformers, are not displayed, for clarity).

Table 3. Relative Free Energies (*G*) of the 15 Conformers at 25 °C in Water, Assuming That the Relative Free Energy of **1T5** is 0

conformer	*G* (kcal/mol)	conformer	*G* (kcal/mol)
1T5	0	**1N9b**[a]	3.7 ± 1.2
1T7	0.3 ± 0.4	**1F3b**[a]	4.0 ± 0.6
1N8	0.7 ± 0.2	**1S10**	4.9 ± 0.9
1N1	1.0 ± 0.8	**1O11**	5.5 ± 0.5
1N6	1.3 ± 0.1	**1F12**	6.1 ± 1.1
1N2b[a]	2.2 ± 1.0	**1S4**	7.3 ± 0.8
1N2	2.4 ± 0.3	**1F3**	9.2 ± 1.4
1N9	2.7 ± 0.9		

[a] See FEP Calculations for Definitions of **1Xb**.

Conformational Stability. The relative free energies of the 15 conformers calculated by the PMF and FEP methods are listed in Table 3. On the basis of the computational study alone, it is predictable that both the tilted T-shaped stacked and

Scheme 1. Syntheses of Compounds **1**−**3** (Free Acids)

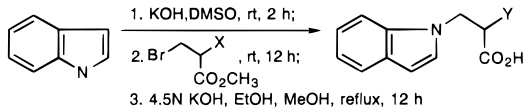

1: X = CH_2Br, Y = Indol-1-yl-methylene; **2:** X = Y = CH_3; **3:** X = Y = H.

nonstacked conformations (**1T5, 1T7**, **1N8**, **1N1**, and **1N6**) are significantly populated in water at 25 °C. Interestingly, according to the inherent accuracy of the PMF and FEP methods, the data suggest that the parallel stacked conformations (**1F12**, **1F3b**, **1S10**, **1S4**, and **1F3**) are not populated. This prompted us to launch experimental studies on **1** to confirm the computational finding.

Synthesis. Compounds **1**−**3** (free acids) were synthesized in low yields (20−30%) by the standard *N*-alkylation method outlined in Scheme 1. The yields encountered were low mainly because elimination of the acidic α proton of the substituted propionate changed, under basic condition, the S_N2 reaction to the low-yield Michael addition.[32] In making **2** and **3**, the retention times of the ester intermediates of **2** and **3** were found identical to that of starting material indole, which caused a purification problem. This problem was avoided by hydrolyzing a mixture of indole and its *N*-substituted ester analogue, followed by extracting the desired acid product with basic solution. Because the NMR spectroscopic studies required only milligrams of the materials, no efforts were made to improve the synthetic yields.

Stacked Interaction in 1. All the aromatic protons of **1**−**3** in D_2O or d_6-DMSO are distinguishable and readily assigned according to Aldrich's proton NMR spectra of different methyl-substituted indole derivatives.[33] The changes in chemical shift of the indole protons of **1**−**3** are listed in Table 4 and depicted in Figure 5. The indole regions of the proton NMR spectra of 1.0 mM **2** and 1.0 mM **3** are essentially identical. The chemical shifts of the aromatic protons of **1** and **2** are independent of concentration over the ranges of 0.01−20 mM and 0.1−40 mM, respectively (Table 4b). Solutions of concentrations higher than 20 mM for **1** and 40 mM for **2** became turbid. These results indicate that intermolecular interactions are insignificant at 0.5 mM **1** and at 1.0 mM **2**. However, the resonances of protons H^6 and H^7 of 0.5 mM **1** in D_2O at 22 °C are significantly shifted upfield by 0.08 and 0.28 ppm, respectively, relative to those of 1.0 mM **2** at the same condition. A smaller upfield shift ($\Delta\delta_{H7} = -0.16$ ppm) was also observed in d_6-DMSO at 22 °C. These results revealed the stacking interaction between the two indole rings of **1** in D_2O and in d_6-DMSO.

Populated Tilted T-Shaped Stacked Conformations. Furthermore, the upfield shifts indicate that protons H^6 and H^7 experience electron shielding. Examination of the Dreiding stereomodel of **1** (page T391, 1997 Aldrich Catalog, 1001 W. St. Paul Ave., Milwaukee, WI 53233) revealed that only the tilted T-shaped stacked conformations (**1T5** and **1T7**) permit spatial arrangements in which H^6 and H^7 are located above the inner region of one indole ring, therefore experiencing electron shielding. The off-center stacked conformers could also render a spatial arrangement in which H^6 and H^7 experience electron shielding. However, this conformation would inevitably result in a downfield shift of H^5, due to the location of H^5 over the outer region of the same indole ring that causes the upfield shifts of H^6 and H^7, but the downfield shift of H^5 was not observed in the spectra of **1**, **2**, and **3** (Table 4 and Figure 5). Therefore, the observation of just the upfield shifts of H^6 and H^7 suggested that the tilted T-shaped conformations (**1T5** and/or **1T7**) are populated in D_2O and in d_6-DMSO, whereas the parallel stacked conformations are not populated.

Populated Nonstacked Conformations. In the NMR spectra of **1** in D_2O and in d_6-DMSO, there are (i) one set of indole proton resonances, (ii) two methylene proton resonances (H_a and H_b), and (iii) a pair of different coupling constants J_{ac} (9 to 8 Hz) and J_{bc} (6 Hz) (Figures 5 and 6 and Table 5). To account for the symmetry of the spectra, the asymmetric conformer **1T7** (**1T5**) must rapidly interchange to its enantiomeric conformer **1T7′** (**1T5′**) by and only by interchange of **1T7** through a symmetric "intermediate" **1N1** (or **1T5** through a symmetric "intermediate" **1N6**) (Figure 6). In this way, the two indole rings over time will experience the same environment; axial proton $H_{a'}$ ($H_{a''}$) in **1T7** (**1T5**) will interchange to equatorial proton $H_{b''}$ ($H_{b'}$) in **1T7′** (**1T5′**) through a 120° rotation of bond T4 (a 120° rotation of bond T2), and it will then interchange to equatorial proton $H_{b''}$ ($H_{b'}$) in **1T7** and/or **1T5** through mirror inversion of **1T7′** (**1T5′**) to **1T7** (**1T5**), consequently reducing four distinct methylene protons in asymmetric **1T7** (**1T5**) to two distinct methylene protons of H_a (an average of $H_{a'}$ and $H_{b''}$) and H_b (an average of $H_{b'}$ and $H_{a''}$). However, interchanges of $H_{a'}$ to $H_{b''}$ and $H_{b'}$ to $H_{a''}$ would result in $J_{ac} = J_{bc}$, since $J_{ac} = (J_{a'c} + J_{b''c})/2$, $J_{bc} = (J_{b'c} + J_{a''c})/2$, $J_{a'c} = J_{a''c}$, and $J_{b''c} = J_{b'c}$. This contradicts the observation of $J_{ac} = 9$ to 8 Hz and $J_{bc} = 6$ Hz. Therefore, **1T5** and **1T5′** and/or **1T7** and **1T7′** cannot be the only populated conformers. To account for the different J_{ac} and J_{bc}, the symmetric "intermediate" **1N1** and/or **1N6** must also be populated so that the observed axial and equatorial protons become approximately $(H_{a'} + H_{b''} + H_{a'''})/3$ and $(H_{b'} + H_{a''} + H_{b'''})/3$, respectively (Figure 6b). Accordingly, J_{ac} approximately equals $(J_{a'c} + J_{b''c} + J_{a'''c})/3 = (9 + 5 + 9)/3 =$ 8 Hz and J_{bc} is about $(J_{b'c} + J_{a''c} + J_{b'''c})/3 = (5 + 9 + 5)/3 =$ 6 Hz, which are now consistent with (i) the upfield chemical shifts of H^6 and H,[7] (ii) the symmetry of the spectra, and (iii) the well-differentiated J_{ac} and J_{bc}. Therefore, the observations of one set of indole proton resonances and two methylene proton resonances and yet a pair of different J_{ac} and J_{bc} suggest that **1N6** and/or **1N1** is also populated in water and in DMSO.

On the basis of the NMR study alone (i.e., independent of the calculated free energies), it is clear that both the tilted T-shaped stacked and nonstacked conformers are populated in water and in DMSO at 22 °C, and they exist in a rapid equilibrium. Although the NMR study provides no insight into the possibility that **1N8** may or may not be populated in water, the experimental study does confirm the computational findings of all other populated conformations (**1T5, 1T7**, **1N1**, and **1N6**).

Hydrophobic Effect. At 22 °C, the upfield shift of H^7 of 0.5 mM **1** in d_6-DMSO was found to be 0.12 ppm less than the corresponding shift in water (Table 4), indicating that population of the nonstacked conformations is larger in d_6-DMSO than in water. This result suggests that the stacking interaction of **1** is weak, but it is stronger in water than in DMSO, consistent with the role expected from the hydrophobic effect. One would observe a larger population of the stacked conformation in d_6-DMSO, whose dielectric constant is smaller than that of water, if the electrostatic interaction were the only driving force of the aromatic stacking interactions. To further support the role of the hydrophobic effect, the NMR studies were carried out at varied temperatures. Interestingly, at 60 °C, only the broadened signal of H^7 of 0.5 mM **1** in water was found shifted upfield by

(32) Doebel, K. J.; Wasley, J. W. F. *J. Med. Chem.* **1972**, *15*, 1081−1082.

(33) Pouchert, C. J.; Behnke, J. *The Aldrich library of 13C and 1H FT-NMR spectra*; Aldrich Chemical: Milwaukee, WI, 1992.

Table 4. Changes in Chemical Shift (ppm) of the Indole Protons ($\Delta\delta_H = \delta_H$ in **1** or **3** $- \delta_H$ in **2**) and (b) Chemical Shifts of the Aromatic Protons of **1** and **2** versus Concentration in D_2O at 22 °C

(a) $\Delta\delta_H$ of Indole Protons

	solvent	*T* (°C)	$\Delta\delta_{H2}$	$\Delta\delta_{H3}$	$\Delta\delta_{H4}$	$\Delta\delta_{H5}$	$\Delta\delta_{H6}$	$\Delta\delta_{H7}$
3 relative to **2**	D_2O	22	−0.01	0.01	0	0	0.01	0
3 relative to **2**	d_6-DMSO	22	−0.02	0.01	0	−0.01	0	0
1 relative to **2**	D_2O	22	−0.02	0.01	0	−0.01	−0.08	−0.28
1 relative to **2**	D_2O	60	−0.06	−0.01	−0.02	−0.03	−0.10	−0.38
1 relative to **2**	d_6-DMSO	22	−0.01	0.02	0	0.01	−0.04	−0.16
1 relative to **2**	d_6-DMSO	60	0	0.02	0.01	0	−0.05	−0.19
1 relative to **2**	d_6-DMSO	100	−0.01	0.02	0	−0.01	−0.06	−0.17

(b) Chemical Shifts of the Aromatic Protons of **1** and **2** versus Concentration in D_2O at 22 °C

	H^4 (ppm)	H^2 (ppm)	H^7 (ppm)	H^6 (ppm)	H^5 (ppm)	H^3 (ppm)
1 (20 mM)	7.54	7.14	7.11	7.05	6.99	6.41
1 (2.0 mM)	7.54	7.16	7.11	7.06	6.99	6.42
1 (1.0 mM)	7.55	7.16	7.11	7.04	7.00	6.43
1 (0.1 mM)	7.55	7.16	7.11	7.06	7.00	6.42
1 (0.01 mM)	7.55	7.17	7.13	7.07	7.02	6.43
2 (40 mM)	7.54	7.17	7.41	7.13	7.00	6.40
2 (20 mM)	7.54	7.17	7.41	7.14	7.00	6.40
2 (2 mM)	7.55	7.18	7.43	7.14	7.00	6.41
2 (1 mM)	7.55	7.18	7.43	7.14	7.00	6.41
2 (0.1 mM)	7.55	7.18	7.43	7.14	7.01	6.42

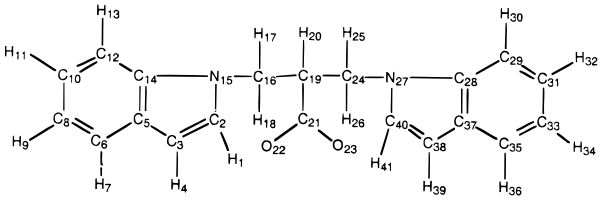

Figure 4. Specifications of the atom identifications of **1**.

0.10 ppm relative to the corresponding sharp signal of H^7 in water at 22 °C (Table 4 and Figures 5 and 7). Other chemical shift changes of **1** are insignificant in comparison with the chemical shift differences between **2** and **3** (Table 4). Signal broadening occurred only to H^6 and H^7 in water at 60 °C. In contrast, a further upfield shift and broadening of H^7 were not observed in d_6-DMSO at 60 °C and even at 100 °C (Table 4 and Figure 7). Such observations indicated that a temperature of 60 °C is not high enough to reduce or abolish the hydrophobic effect of **1** in water. The results, therefore, suggest that stacked conformers such as **1T5** and **1T7** become more populated at 60 °C in water. Clearly, elevating the temperature to 60 °C increased the stacked conformations in water and not in d_6-DMSO. This further suggests that the hydrophobic effect plays a role in the stacking interaction of **1**.

Discussion

In an attempt to provide additional links between the NMR experimental results and the computational predictions, we back-calculated the chemical shifts of **2** and **3** using the ab initio method with the B3LYP/6-31G*//B3LYP/6-31G* function, employing the Gaussian 94 program (see Materials and Methods).[34] The calculated chemical shifts of relatively large and flexible structures **2** and **3** are in good agreement with experimentally measured values (Table 6). However, the difference (0.76 ppm) in the calculated chemical shift of H^7 between **2** and **3** is larger than the observed change (0.28 ppm) of H^7 in **1** caused by electron shielding in the conformations with intra-aromatic interactions. This result, unfortunately, precludes a meaningful analysis of the chemical shifts in **1**.

(34) *Gaussian 92 and 94*; Gaussian, Inc.: Pittsburgh, PA 1992.

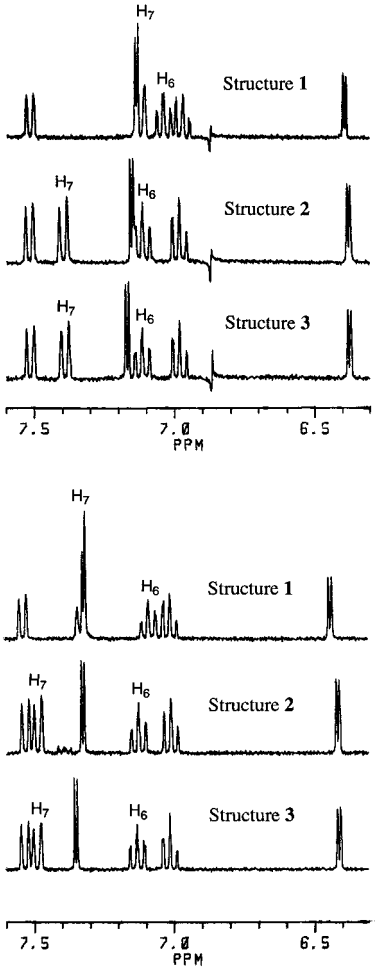

Figure 5. Comparison of the chemical shifts of the aromatic protons among **1** (0.5 mM), **2** (1.0 mM), and **3** (1.0 mM) in D_2O (top) and d_6-DMSO (bottom) at 22 °C.

Back-calculation of NOE spectra of **1** in different conformations may also, in theory, provide a link between the experiments and the calculations. However, the NOE back-calculation was not pursued because of the symmetrical nature of the observed

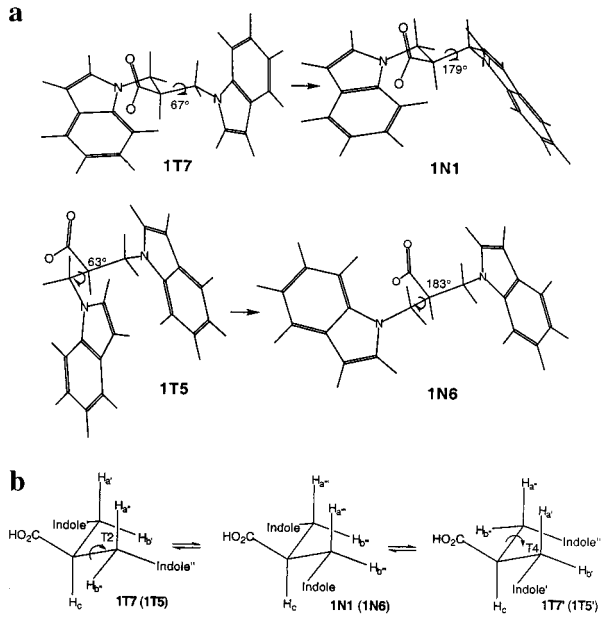

Figure 6. (a) Conformational interconversions of **1T7** to **1N1** and **1T5** to **1N6**. (b) Schematic representation of the conformational interconversions that interchange Ha′ to Hb″ and Hb′ to Ha″, and yet differentiate J_{ac} from J_{bc}.

Table 5. Coupling Constants of the Methylene Protons in 0.5 mM **1** and 1.0 mM **2**

structure	solvent	T (°C)	J_{ac} (Hz)	J_{bc} (Hz)	J_{ab} (Hz)
1	D_2O	22	9	6	14
1	D_2O	60	8	na[a]	14
1	d_6-DMSO	22	9	6	14
1	d_6-DMSO	60	8	6	14
1	d_6-DMSO	100	8	7	14
2	D_2O	22	8	7	14
2	D_2O	60	7	na[a]	14
2	d_6-DMSO	22	7	7	14
2	d_6-DMSO	60	7	7	14

[a] Not available because the signal was overlapped by the solvent signal.

spectrum of **1**. In practice, the molecular symmetry of **1** causes the complication in distinguishing the NOE signals between two aromatic protons in one indole ring from the ones between two protons in two indole rings in the experimentally measured spectra and also the complication in averaging the NOE signals in the back-calculation.

There are a large number of structural precedents for heterocycles to adopt parallel stacked conformations.[12,13,17,19] It is also well known that the nucleotide bases tend to adopt parallel stacked conformations in ordered DNA and RNA structures.[35] The tilted T-shaped stacked conformations are reportedly seen only in aromatic hydrocarbons.[21,36−38] We found from both computational and experimental studies that the parallel stacked conformations of bis-indole **1** are not populated in water, but rather, the molecule is in an equilibrium between the tilted T-shaped stacked and nonstacked conformations. This unprecedented observation does not imply that nucleotide bases tend to adopt the tilted T-shaped conformation, because the charges

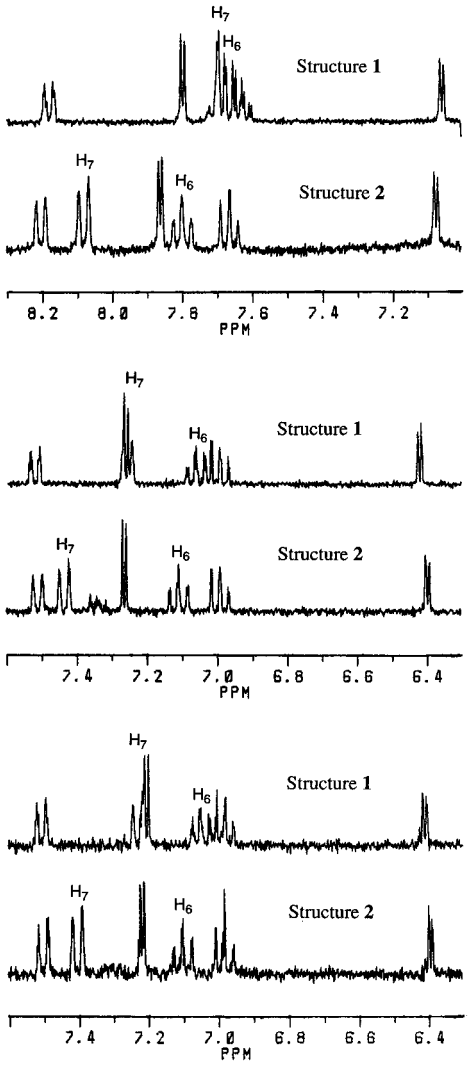

Figure 7. Comparison of the chemical shifts of the aromatic protons among **1** (0.5 mM) and **2** (1.0 mM) in D_2O at 60 °C (top) and in d_6-DMSO at 60 °C (middle), and in d_6-DMSO at 100 °C (bottom).

Table 6. Observed and Calculated Chemical Shifts of the Aromatic Protons in **2** and **3**

	chemical shift (ppm)					
	H^2	H^3	H^4	H^5	H^6	H^7
Structure **2**						
observed in DMSO	7.31	6.40	7.52	6.99	7.11	7.47
observed in D_2O	7.15	6.38	7.51	6.98	7.12	7.39
B3LYP/6-31G*// B3LYP/6-31G*	7.67	5.69	6.91	6.50	6.62	7.83
Structure **3**						
observed in DMSO	7.33	6.39	7.52	7.00	7.11	7.47
observed in D_2O	7.16	6.37	7.51	6.98	7.11	7.39
B3LYP/6-31G*// B3LYP/6-31G*	7.71	5.67	6.96	6.71	6.60	7.07

of the indole ring are different from those of nucleotide bases and, more importantly, because the linker of **1** is different from those used to restrain the nucleotide bases in DNA and RNA. In addition, the driving force to form parallel stacked nucleotide bases in DNA and RNA is not necessarily the same as the one to adopt the tilted T-shaped stacked indole pair in **1**. The hydrophobic effect simply arises from stronger solvent−solvent than solvent−solute interactions. This effect on aromatic stacking interactions needs careful evaluation. In the present study, examining the chemical shift changes alone would lead to a

(35) Bugg, C. E.; Thomas, J. M.; Sundaralingam, M.; Rao, S. T. *Biopolymers* **1971**, *10*, 175−219.
(36) Janda, K. C.; Hemminger, J. C.; Winn, J. S.; Novick, S. E.; Harris, S. J.; Klemperer, W. *J. Chem. Phys.* **1975**, *63*, 1419.
(37) Cox, E. G.; Cruikshank, D. W. J.; Smith, J. A. C. *Proc. R. Soc. London* **1958**, *A247*, 1.
(38) Paliwal, S.; Geib, S.; Wilcox, C. S. *J. Am. Chem. Soc.* **1994**, *116*, 4497−4498.

conclusion that only the stacked conformation(s) is populated in D_2O as well as in d_6-DMSO, since the changes of chemical shifts provide no indication of whether the nonstacked conformations are also populated. This would lead to a wrong conclusion that the hydrophobic effect has nothing to do with stacking interactions. However, combining the chemical shift changes with the calculated free energies of various conformations in water at 25 °C (Table 3), the symmetry of the NMR spectra, and the observed and back-calculated coupling constants led to the interpretation that both the tilted T-shaped stacked and nonstacked conformations are populated in D_2O and in d_6-DMSO, and they are in a rapid equilibrium. Given the fact that both the tilted T-shaped and nonstacked conformations are populated in both D_2O and d_6-DMSO, it is clear that the stacking interaction in **1** is weak. Nevertheless, the importance of the hydrophobic effect in the weak stacking interactions of **1** is supported by the facts that the percentage of the stacked conformation of **1** in water is higher than that in organic solvent at 22 °C, and that the percentage difference is magnified at 60 °C, which is consistent with the fact that the hydrophobic effect is often an entropy-driven process. In contrast, refs 9−11 suggested that **4** was parallel stacked and **5** nonstacked based on the NMR studies and concluded that the hydrophobic effect does not play a role in aromatic stacking, since the polar **4** stacked and the nonpolar **5** did not.[9−11] Our preliminary free energy calculations mutating **1** to **4** suggest that the tilted T-shaped stacking conformations should be considered in the interpretation of experimental data on **4**, but these are not yet definitive. In any case, our results on **1** stand on their own in showing the importance of the hydrophobic effect on aromatic association in water and suggesting that caution should be used in design of simplified molecular probes to study the structures and functions of complicated proteins and nucleic acids.

Materials and Methods

Synthesis. Methyl (2,2)-Bis(indol-1-yl-methyl)acetate. A mixture of indole (500 mg) and powdered 85% KOH (350 mg) in dry DMSO (6.0 mL) was stirred at room temperature (RT) for 2 h under argon. Methyl 3-bromo-2-(bromomethyl)propionate (300 μL) was then added dropwise to the bluish solution at RT. The reaction was quenched after 20 h of stirring at RT. The extract of CH_2Cl_2 was washed with saturated aqueous NH_4Cl and dried over $MgSO_4$. Flash column chromatography on silica gel using 10% EtOAc in hexane as eluent gave 140 mg (20%) of the ester product as a yellowish oil: R_f = 0.47 (20% EtOAc in hexane); IR ($CDCl_3$) 3054, 2951, 1732, 1514, 1454, 1314, 1263, 1213, 1177, and 741 cm^{-1}; ^{1}H NMR ($CDCl_3$) δ 7.62 (d, J = 9.0 Hz, 2 H), 7.15−7.02 (m, 8 H), 6.50 (dd, J = 3.0, 6.0 Hz, 2 H), 4.51 (dd, J = 9.0, 15.0, 2 H), 4.18 (dd, J = 6.0, 15.0 Hz, 2 H), and 3.57−3.48 (m, 4 H); ^{13}C NMR ($CDCl_3$) δ 172.5, 135.8, 128.7, 127.9, 122.0, 121.2, 119.8, 109.0, 102.2, 52.3, 47.3, and 45.7; MS (70 eV) m/z 332 (M^+), 170, 130, 103, 77, and 63; HRMS (ESI), m/z calcd for $C_{21}H_{21}N_2O_2$ ($M + H^+$) 333.1603, found 333.1600.

(2,2)-Bis(indol-1-yl-methyl)acetic Acid. KOH (4.5 N, 8 mL) was added dropwise at RT to a solution of methyl (2,2)-bis(indol-1-yl-methyl)acetate (500 mg) in 10 mL of MeOH and 8 mL of EtOH. The resulting solution was refluxed under argon for 12 h and poured into 50 mL of water. The alcohol in the resulting mixture was removed by rotary vaporation under reduced pressure. The aqueous solution was first washed with EtOAc and then adjusted to pH 5 with 2 N HCl. The product was extracted with EtOAc and dried over $MgSO_4$. Flash column chromatography on silica gel using first 30% EtOAc in hexane as eluent to remove impurities and then EtOAc as eluent yielded 450 mg (94%) of the acid product as a reddish solid: mp 132−133 °C; IR ($CDCl_3$) 3063, 2928, 1715, 1516, 1458, 1317, 1227, 1177, 907, and 733 cm^{-1}; ^{1}H NMR ($CDCl_3$) δ 10.38 (s, 1 H), 7.63−7.57 (m, 2 H), 7.11−7.05 (m, 4 H), 6.79−6.93 (m, 4 H), 6.48 (d, J = 3.0 Hz, 2 H), 4.39 (dd, J = 6.0, 15.0 Hz, 2 H), 4.04 (dd, J = 6.0, 15.0 Hz, 2 H), and 3.50−3.42 (m, 1 H); ^{13}C NMR ($CDCl_3$) δ 177.9, 135.7, 128.6, 127.8, 122.0, 121.2, 119.9, 108.9, 102.4, 47.2, and 45.2; HRMS (ESI), m/z calcd for $C_{20}H_{19}N_2O_2$ ($M + H^+$): 319.1446, found 319.1446.

3-Indol-1-yl-2-methylpropionic Acid. A mixture of indole (500 mg) and powdered 85% KOH (350 mg) in 6.0 mL of dry DMSO was stirred at RT for 2 h under argon. Methyl 3-bromo-2-methylpropionate (680 μL) was then added dropwise to the bluish solution at RT. The reaction was quenched after 20 h of stirring at RT. The extract of CH_2Cl_2 was washed with saturated aqueous NH_4Cl and dried over $MgSO_4$. Flash column chromatography on silica gel using 10% EtOAc in hexane as eluent gave a mixture of the desired intermediate and indole. KOH (4.5 N, 8 mL) was added dropwise at RT to a solution of 400 mg of the mixture of the propionate intermediate and indole in 10 mL of MeOH and 8 mL of EtOH. After 12 h of refluxing under argon, the desired acid product as a yellowish solid (326 mg, 30% yield) was isolated by a procedure similar to that used in isolating (2,2)-bis(indol-1-yl-methyl)acetic acid: mp 59−61 °C; IR ($CDCl_3$) 3098, 3054, 2978, 2940, 2882, 1707, 1452, 1314, 1236, 1204, and 741 cm^{-1}; ^{1}H NMR ($CDCl_3$) δ 11.94 (s, 1 H), 7.60 (d, J = 9.0 Hz, 1 H), 7.28 (d, J = 6.0 Hz, 1H), 7.19−7.14 (m, 1 H), 7.10−6.99 (m, 2 H), 6.45 (d, J = 3.0 Hz, 1 H), 4.38 (dd, J = 6.0, 12.0 Hz, 1 H), 4.00 (dd, J = 9.0, 15.0 Hz, 1 H), 3.00−2.93 (m, 1 H), and 1.21 (d, J = 6.0 Hz, 3 H); ^{13}C NMR ($CDCl_3$) δ 180.9, 135.9, 128.6, 128.2, 121.6, 121.0, 119.5, 109.2, 101.6, 48.4, 40.4, and 14.9; HRMS (ESI), m/z calcd for $C_{12}H_{14}NO_2$ ($M + H^+$) 204.1024, found 204.1020.

3-Indol-1-yl-propionic Acid. A procedure similar to that employed in the synthesis of 3-indol-1-yl-2-methylpropionic acid yielded the desired product (30%) as a yellowish solid: mp 87−88 °C; IR ($CDCl_3$) 3052, 2915, 1715, 1462, 1316, 1238, 1179, 928, and 746 cm^{-1}; ^{1}H NMR ($CDCl_3$) δ 11.04 (s, 1 H), 7.58 (d, J = 6.0 Hz, 1 H), 7.21−7.03 (m, 3 H), 6.96 (d, J = 3.0 Hz, 1 H), 6.42 (d, J = 3.0 Hz, 1 H), 4.19 (t, J = 6.0 Hz, 2 H), and 2.64 (t, J = 9.0 Hz, 2 H); ^{13}C NMR ($CDCl_3$) δ 177.6, 135.5, 128.6, 127.7, 121.6, 121.0, 119.5, 108.9, 101.6, 41.1, and 34.4; HRMS (ESI), m/z calcd for $C_{11}H_{12}NO_2$ ($M + H^+$) 190.0868, found 190.0861.

General Description of the Computational Studies. All the calculations were performed by employing the AMBER 4.1 program (various minor revisions made from October 1994 to March 1997) with the Cornell et al. all-atom force field and by using the Gaussian 92 program.[23,28,34] All the MD, PMF, and FEP calculations used (i) the SHAKE procedure for all bonds of the system,[39] (ii) a time step of 1.0 fs, (iii) a dielectric constant ϵ_0 = 1.0, (iv) a cutoff distance of 9.0 Å for calculating nonbonded interactions, (v) a rectangular periodic boundary condition with the constant temperature (T = 298 K and TAUTP = 0.3) and constant pressure (P = 1 atm and TAUP = 0.3) algorithm, (vi) the Berendsen coupling algorithm (NTT = 1),[40] and (vii) a flag (IFTRES = 0) to calculate all solute−solute nonbonded interactions. The nonbonded list was updated every 25 steps in the MD simulations and the PMF calculations.

Structure **1** was built with two MEN (1-methyleneindole) residues and one ACT ($CHCO_2^-$) residues with the PREP, LINK, EDIT, and PARM modules of the AMBER program. For all the MD and PMF calculations, one negatively charged molecule **1** and one sodium counterion were solvated by the TIP3P water molecules in a periodic boundary box (DISO = 2.2, DISH = 2.0, NCUBE = 4, CUTX = 10.0, CUTY = 13.0, CUTZ = 14.0, generally a box size of 32 × 33 × 35 Å^3 with about 1050 water molecules; note that the number of water molecules varies with conformations of **1**). The resulting system was slowly heated to 298 K (1 K per 100 steps) by coupling to different heat baths with constant NTV simulation and then equilibrated with constant NTP simulation for 50 ps at 298 K and 1 atm.

For all the FEP and PMF calculations, (i) the thermodynamic integration approach was used; (ii) the reported free energy change of a perturbation or a subperturbation was a mean of the free energy changes calculated in forward and reverse runs plus and minus the standard deviation of the mean; (iii) the reported free energy change of a perturbation which was broken into several subperturbations was

(39) Ryckaert, J. P.; Ciccotti, G.; Berendsen, H. J. C. *J. Comput. Phys.* **1977**, *23*, 327−341.

(40) Berendsen, H. J. C.; Postma, J. P. M.; van Gunsteren, W. F.; Di Nola, A.; Haak, J. R. *J. Chem. Phys.* **1984**, *81*, 3684−3690.

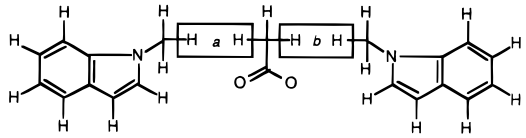

Figure 8. Splicing scheme used for deriving the charges of **1**.

a sum of the free energy changes of the subperturbations plus and minus a sum of the corresponding standard deviations; and (iv) convergence of each perturbation was checked by the criterion that the difference in free energy change between a run and the run calculated with doubled simulation time should not be greater than the standard deviation, otherwise longer simulation was performed until the criterion was met.

RESP Charges. Using the RESP module of the AMBER program, the RESP charges of **1** were derived by splicing the electrostatic potentials of two 1-methylindole and one deprotonated acetic acid. A two-stage fitting protocol was used. The Lagrange constraints were used to set a net charge of the four extra protons outlined in boxes a and b equal to zero, leaving a net charge of all atoms of **1** equal to −1 (see Figure 8).[28,41] The electrostatic potentials of MEN and ACT were generated by the ab initio calculations with the RHF/6-31G*//RHF/6-31G* function employing the Gaussian 92 program.[34] The splicing approach was used to reduce the conformational influence on the charge calculation.

Conformational Analysis. A total of 1296 different conformers were generated by specifying all discrete possibilities at 60° of arc increment in a range of 0−360° for the first four torsions (T1−T4) defined in Table 1. Conformers were optimized without restraining any torsions during the energy minimization by employing the Sander module.[23,28] Based on the criterion that two conformers are different if the difference of one of the four defined torsions between the two conformers is greater than 30° of arc, conformational cluster analysis on the optimized conformers resulted in 38 different conformers. Duplicated structures and mirror images due to the symmetric nature of **1** were deleted by visual inspection, which yielded 12 different conformers. The relative orientation of the carboxylate group was not taken into account in order to make use of FEP calculations.

MD Simulations. For all the 1.0 ns MD simulations, the first four specified torsions of **1** (Table 1) were calculated from all the trajectories saved at every 1.0-ps interval using the CARNAL module of the AMBER program. A table of such torsions was analyzed to obtain information about the conformational changes. One compares such torsions with 38 sets of the torsions that were obtained initially from the conformational search and designates one or none of the 12 conformers that is identical to the instantaneous conformer of **1** at 1.0-ps intervals, according to the criterion that two conformers are identical if the differences of the four torsions between the two conformers are all less than 30° of arc.

Conformer **1S10** and its thermodynamically identical mirror image **1S10′** were arbitrarily chosen in the first two simulations. Analysis of all trajectories collected at 1.0-ps intervals during the 1.0-ns MD simulation revealed that **1S10** was stable only for 2.0 ps and then changed to **1S4**, which was stable for 203.0 ps and then changed to **1O11**, which was stable for 565.0 ps and then changed to **1T7**, which was stable for 229.0 ps until the simulation stopped (see Table 7). In the simulation with **1S10′**, **1S10′** was immediately changed to "intermediate" **1N2** and later to other "intermediates" (see Table 7). Conformers **1T7** and **1N2**, which appeared at the end of the first two simulations, were then chosen in the next two simulations. The simulation with the conformer that appeared at the end of the prior simulation was iterated until a reasonably stable conformer such as **1T5** was identified, or until the conformer that appeared at the end of a simulation was identical to the conformers that appeared previously in the same or other simulations. Other conformers, which did not appear in the previous simulations, were arbitrarily chosen again in a new simulation, followed by subsequent simulations with the conformers that appeared at the end of the former simulations. This process was repeated until all 12 conformers had appeared in the simulations.

(41) Cieplak, P.; Cornell, W. D.; Bayly, C.; Kollman, P. A. *J. Comput. Chem.* **1995**, *16*, 1357−1377.

Table 7. Observed Interconversions among the 12 Conformers in the MD Simulations and Their Duration in Water at 25 °C

1S10 (2 ps) → **1S4** (203 ps) → **1O11** (565 ps) → **1T7** (229 ps/stop)

1S10′ (0 ps) → **1N2** (263 ps) → **1S10** (46 ps) → **1N9** (47 ps) → **1N1** (39 ps) → **1N8** (17 ps) → **1N1** (209 ps) → **1N9** (94 ps) → **1N1** (183 ps) → **1N8** (2 ps) → **1N1** (6 ps) → **1N8** (15 ps) → **1N2** (79 ps/stop)

1T7 (213 ps) → **1N1** (311 ps) → **1T7** (171 ps) → **1N1** (305 ps/stop)

1N2 (225 ps) → **1T5** (775 ps/stop)

1N1 (17 ps) → **1N6** (522 ps) → **1N8** (7 ps) → **1N6** (30 ps) → **1N8** (2 ps) → **1N6** (41 ps) → **1N2** (222 ps/stop)

1S4 (379 ps) → **1N2** (384 ps) → **1N9** (237 ps/stop)

1F12 (7 ps) → **1S10** (52 ps) → **1N2** (50 ps) → **1N8** (1 ps) → **1N6** (7 ps) → **1N8** (41 ps) → **1N2** (331 ps) → **1T7** (511 ps/stop)

1T7 (334 ps) → **1N6** (492 ps) → **1T5** (508 ps/stop)

1F3 (0 ps) → **1O11** (353 ps) → **1T7** (65 ps) → **1N2** (58 ps) → **1T5** (524 ps/stop)

1N9 (388 ps) → **1O11** (48 ps) → **1T5** (463 ps) → **1N9** (101 ps/stop)

1N8 (0 ps) → **1N6** (44 ps) → **1N8** (4 ps) → **1N6** (25 ps) → **1N8** (1 ps) → **1N6** (2 ps) → **1N8** (6 ps) → **1N6** (14 ps) → **1N8** (4 ps) → **1N6** (9 ps) → **1N8** (3 ps) → **1N6** (61 ps) → **1N8** (12 ps) → **1N6** (15 ps) → **1N8** (13 ps) → **1N6** (1 ps) → **1N8** (3 ps) → **1N6** (7 ps) → **1N8** (5 ps) → **1N6** (11pa) → **1N8** (6 ps) → **1N6** (12 ps) → **1N8** (15 ps) → **1N6** (47 ps) → **1N8** (4 ps) → **1N6** (3 ps) → **1N8** (8 ps) → **1N6** (91 ps) → **1N8** (3 ps) → **1N6** (7 ps) → **1N8** (5 ps) → **1N6** (40 ps) → **1N8** (2 ps) → **1N6** (1 ps) → **1N8** (4 ps) → **1N6** (7 ps) → **1N8** (9 ps) → **1N6** (3 ps) → **1N8** (1 ps) → **1N6** (6 ps) → **1N8** (20 ps) → **1N6** (17 ps) → **1N8** (5 ps) → **1N6** (10 ps) → **1N8** (5 ps) → **1N6** (119 ps) → **1N8** (9 ps) → **1N1** (36 ps) → **1N8** (17 ps) → **1N6** (1 ps) → **1N8** (1 ps) → **1N6** (85 ps) → **1T5** (161 ps/stop)

PMF Calculations. For effective sampling, the observed interconversions among the 12 conformers in the MD simulations in water at 25 °C were used as conformational perturbation paths in the PMF calculations. This is crucial to the PMF calculations. In theory, the calculated free energy change does not depend on paths of perturbations along which the calculation is performed. In practice, due to limitation in sampling, such a calculation can often be path-dependent. The PMF calculations with two arbitrarily selected conformers often yielded huge hysteresis caused by close van der Waals contacts incurred during the conformational change from one state to the other. Pilot studies showed that using two conformers that were found to be directly interconvertible in the MD simulation can minimize the problem of the close van der Waals contacts. Electrostatic and van der Waals contributions were simultaneously calculated with 100 windows. Each forward or reverse run was calculated for at least 1.0 ns. All conformational perturbation paths were visually inspected with the Midas Plus graphics program of the UCSF Computer Graphics Lab to ensure that no close van der Waals contacts incurred in the conformational changes. For a smooth conformational transition, some of the PMF calculations listed in Table 8 were broken into two subperturbations which change part of the four torsions at the first step and the rest at the last step. The free energy changes of 12 independent perturbations are listed in Table 8. The convergence of the data in Table 8 is demonstrated by the fact that the free energy difference (0.3 ± 0.4 kcal/mol) of the perturbation of **1T5** to **1T7** matches the free energy difference (0.4 ± 0.6 kcal/mol) of two consecutive perturbations from **1T5** to **1T7** through **1N6**.

FEP Calculations. All derivative conformers generated by exchanging the carboxylate group with the methine proton (i.e., **1N2b**, **1F3b**, and **1N9b**, see Figure 9), excluding those whose potential energy is 5 kcal/mol higher than that of the corresponding parent conformers, were then compared for free energy difference at 25 °C in water with their parent conformers. This free energy difference was computed by the FEP method.[22]

In the FEP calculation, the conformation of isobutyric acid was restrained (rigidified) with a harmonic potential (IFCON = CONS and

Table 8. Free Energy Differences between Different Conformations at 25 °C in Water

perturbation	ΔG (kcal/mol)	time (ns)
1N6 to **1N6′int**	4.8 ± 0.3	8.0
1T7 to **1N1**	0.7 ± 0.4	8.2
1T7 to **1T5**	-0.3 ± 0.4	6.0
1N9 to **1O11**	2.8 ± 0.4	2.0
1T7 to **1O11**	5.2 ± 0.07	2.0
1S10 to **1S4**	2.4 ± 0.1	2.0
1S4 to **1O11**	-1.8 ± 0.3	2.0
1N2 to **1N6**	-1.1 ± 0.2	4.4
1N8 to **1N6**	0.6 ± 0.07	3.2
1N6 to **1T5**	-1.3 ± 0.07	4.0
1S10 to **1F12**	1.2 ± 0.2	2.0
1T7 to **1F3b**	3.7 ± 0.2	2.0
1N6 to **1T7**	-0.9 ± 0.5	4.0

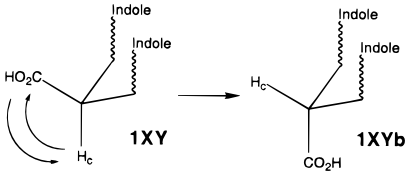

Figure 9. Conformational derivation by exchanging the carboxylate group with the methine proton.

Table 9. Free Energy Differences at 25 °C in Water between the Parent and Derivative Conformers Restrained by the Force Constant of 800 kcal/mol

perturbation	ΔG (kcal/mol)	time (ns)
1N6′int to **1N6′**	-4.4 ± 0.4	16.0
1N2 to **1N2b**	-0.2 ± 0.7	8.0
1F3 to **1F3b**	-5.2 ± 0.8	8.0
1N9 to **1N9b**	1.0 ± 0.3	8.0

CONK = 800 kcal/mol in PARM). The perturbation was broken into two subperturbations in order to avoid calculation failure due to the presence of two negatively charged intermediate carboxylate groups in a one-step perturbation. The first subperturbation mutated the carboxylate group to a methine proton. The second then changed the other methine proton to a carboxylate group. Electrostatic and van der Waals contributions were separately calculated with 1000 windows for electrostatic and 50 windows for van der Waals. No counterion was included, to avoid calculation failure when the counterion occasionally moved out of the water box after removal of the charges of the carboxylate group. The flag NCORC was set to 1 to calculate the contributions to the free energy from any constraint whose equilibrium value changed with λ.[42] Each forward or reverse run was calculated for at least 1.0 ns. The nonbonded list was updated at every five steps in the FEP calculations.

The results of the FEP calculations are listed in Table 9. Exchange of the carboxylate group with the methine proton makes **1N2** and **1F3** more stable in water by 0.2 ± 0.7 and 5.2 ± 0.8 kcal/mol, respectively. To the contrary, the exchange of the carboxylate group makes the nonstacked conformer **1N9** less stable in water by 1.0 ± 0.3 kcal/mol.

A calculation with different force constants used to restrain the isobutyric acid linker was carried out to examine the effect of the force constant on free energy. The results in Table 10 indicate that changing the force constant from 800 to 8 kcal/mol does not significantly affect the calculated free energy difference. To examine perturbation path efficiency, a calculation with an alternative path was performed. This path consisted of three steps: First, the electrostatic run mutated simultaneously (i) the charge of the methine proton to the charge of carbonyl carbon, (ii) the charge of the carbonyl carbon to the charge of the methine proton, and (iii) the charges of the two oxygen atoms to zero. Second, the van der Waals run exchanged the carboxylate group with the methine proton. Third, the electrostatic run introduced the charges of the two oxygen atoms at the final state. The nonbonded list was updated at every step in this path. The comparison of the free energy changes calculated with the two approaches is listed in Table 11. To achieve a comparable standard deviation of the mean, the three-step path requires less simulation time and is more efficient than the two-step path.

(42) Pearlman, D. A.; Kollman, P. A. *J. Chem. Phys.* **1991**, *94*, 4532−4545.

Table 10. Effect of the Force Constant Used To Restrain the Conformation of **1F3b** on Free Energy at 25 °C in Water

K (kcal/mol)	ΔG (kcal/mol)	time (ns)
800	-5.2 ± 0.8	8.0
8	-5.8 ± 0.6	1.2

Table 11. Free Energy Changes of **1F3** to **1F3b** Calculated with Different Perturbation Approaches at 25 °C in Water

perturbation	ΔG (kcal/mol)	time (ns)
approach 1	-5.2 ± 0.8	8.0
approach 2	-5.3 ± 0.8	6.0

Chemical Shifts of 2 and 3. A total of 14 different conformations for **2** were generated by the same procedure used to generate the different conformations of **1**, except that the orientation of the carboxylate group was taken into account. Similarly, five conformations for **3** were obtained from the conformational search. Optimization using the Gaussian 94 program with the B3LYP/6-31G* function reduced the numbers of different conformations of **2** and **3** to 10 and 3, respectively. The chemical shifts in Table 6 are the average of the chemical shifts of different conformations calculated with the B3LYP/6-31G*//B3LYP/6-31G* function and are relative to the absolute shielding value of tetramethylsilane (32.184025 ppm) calculated with the same function.

Acknowledgment. P.A.K. is pleased to acknowledge research support from the NSF (CHE-9417458). Y.P.P. acknowledges the support of the Mayo Foundation for Medical Education and Research, the help of Drs. Bert E. Thomas IV, Piotr Cieplak, and Christopher Chipot in the charge calculations, and the assistance from the members of the Kollman group in using the AMBER programs. We thank Professor Paul Carlier of the Hong Kong University of Science and Technology for comments on our NMR studies, M. Stacy of the Mayo Foundation for the support of the computing resources at Mayo Clinic Rochester, and L. Benson of the Mayo Foundation for mass spectroscopic analysis. We are grateful to the UCSF Computer Graphics Lab (RR-1081, T. Ferrin, P.I.) for graphics support and to the San Diego and Pittsburgh Supercomputer Center for computational support.

Supporting Information Available: General description of synthesis; NMR spectral data of **1**−**3** in D_2O and d_6-DMSO at different temperatures; Tables I−V containing the atom types, RESP charges, force field parameters of **1**, and Tables VI and VII containing the torsions that define the different conformers of **2** and **3** and the corresponding conformational energies calculated with the B3LYP/6-31G*//B3LYP/6-31G* function (PDF). This material is available free of charge via the Internet at http://pubs.acs.org.

JA9828410